

# Heterogeneous Graph Neural Networks for End-to-End Traffic Assignment and Traffic Flow Learning

Tong Liu<sup>a</sup>, Hadi Meidani<sup>1a</sup>

<sup>a</sup>University of Illinois, Urbana-Champaign, Department of Civil and Environmental Engineering, 205 N Mathews Ave, Urbana, 61801, IL, USA

---

## Abstract

The traffic assignment problem is one of the significant components of traffic flow analysis for which various solution approaches have been proposed. However, deploying these approaches for large-scale networks poses significant challenges. In this paper, we leverage the power of heterogeneous graph neural networks to propose a novel data-driven approach for end-to-end traffic assignment and traffic flow learning. Our model integrates an adaptive graph attention mechanism with auxiliary "virtual" links connecting origin-destination node pairs. This integration enables the model to capture spatial traffic patterns across different links. By incorporating the node-based flow conservation law into the overall loss function, the model ensures the prediction results in compliance with flow conservation principles, resulting in highly accurate predictions for both link flow and flow-capacity ratios. We present numerical experiments on urban transportation networks and show that the proposed heterogeneous graph neural network model outperforms other conventional neural network models in terms of convergence rate and prediction accuracy. Notably, by introducing two different training strategies, the proposed heterogeneous graph neural network model can also be generalized to different network topologies. This approach offers a promising solution for complex traffic flow analysis and prediction, enhancing our understanding and management of a wide range of transportation systems.

*Keywords:* traffic assignment problem, graph neural network, traffic flow prediction, flow conservation, heterogeneous graph

---

## 1. Introduction

Traffic assignment plays a significant role in transportation network analysis. Solving the traffic assignment problem (TAP) enables a deeper understanding of traffic flow patterns and provides insights into traffic congestion (Nie et al., 2004). Traffic congestion is a major concern in urban areas, leading to increased travel times, fuel consumption, and environmental pollution. By identifying the bottlenecks in transportation networks, city planners can make a strategic plan to increase road capacities to mitigate traffic congestion. To this end, the primary objective of the traffic assignment problem is to determine the traffic flow distribution and identify traffic bottlenecks on a given road network. For solving traffic assignment problems, there are two major formulations with different assumptions: (1) the user equilibrium (UE) assignment and (2) the system optimum (SO) assignment. The UE assignment identifies an equilibrium state in which drivers between each origin-destination (OD) pair cannot reduce travel costs by unilaterally shifting to another route (Kuang et al., 2021). On the other hand, in the SO assignment, drivers choose the routes collaboratively so that the total system travel time is minimized (Seliverstov et al., 2017).

Traffic assignment problems have appeared in other transportation engineering problems. For instance, city planners leverage traffic assignment to evaluate the network performance under extreme event scenarios, including hurricanes (Zou and Chen, 2020) and earthquake (Silva-Lopez et al., 2022; Liu and Meidani, 2023a). These evaluations ensure the transportation infrastructure aligns with the city's evolving needs and requirements. Furthermore, the UE-TAP is employed in road network design and retrofit investment optimization as a lower-level constraint in a bi-level optimization problem (Hu et al., 2021; Madadi and de Almeida Correia, 2024).

---

<sup>1</sup>Corresponding Author, meidani@illinois.edu

As a critical preliminary step in setting up the TAPs, it is essential to first obtain accurate origin-destination demands that reflect the realistic travel demands. Multiple research has been proposed to estimate regional OD demands (Zhang et al., 2020; Tang et al., 2021; Zhang et al., 2021), leveraging data from various sensors. Despite these methodological advancements, practical challenges persist. Specifically, sensor failures and malfunctions can impose a significant loss of relevant and reliable OD demand information (Sun et al., 2022). Consequently, the inaccurate estimation of OD demand will hinder the accurate calculation of traffic flows. This issue underscores a research gap in effectively solving TAPs and estimating traffic flows under inaccurate OD demand scenarios. In order to solve TAPs, various efficient algorithms have been proposed (Nie et al., 2004; Di Lorenzo et al., 2015). Despite these advances, it is still computationally demanding to conduct a robust network planning for large-scale networks, when multiple relevant scenarios are considered. This highlights the need to develop scalable solution approaches for TAPs to accommodate diverse network scenarios. In recent years, data-driven approaches have leveraged the availability of large-scale transportation data in various transportation problems. For instance, Ye et al. (2019) combines convolutional neural networks to predict multiple transportation demands using real-world taxi and shared bike demand data. Furthermore, recurrent neural networks (RNNs) have been applied to different prediction tasks in transportation engineering (Zhaowei et al., 2020; Fang et al., 2022). Also, Liu et al. (2023) proposed an implicit neural network to travel choice preferences and equilibrium state modeling from multi-day link flow observations.

Recently, graph neural networks (GNNs) have emerged as a powerful tool in transportation performance analysis since they propagate the node features through a graph structure. Compared with RNNs and CNNs, a key advantage of GNNs is their ability to capture spatial and relational information inherent in transportation networks. Among the recent works, Nishi et al. (2018) developed a traffic signal control algorithm based on graph convolutional networks and reinforcement learning. Liu and Meidani (2022) utilizes a graph convolutional network to analyze the node-to-node accessibility of regional transportation systems under earthquakes. Despite these advancements in neural networks, the literature on applying neural networks to TAPs remains relatively sparse. Fan et al. (2023) integrated CNNs with RNNs for predicting the traffic flow distribution by considering the transportation network as the grid map. Furthermore, Rahman and Hasan (2023) utilizes the graph convolutional network for solving UE-TAP and predicting the traffic flow pattern. However, the aforementioned model encountered a few limitations. First of all, one major limitation of the grid-based CNN model (Fan et al., 2023) is that it cannot fully capture the topologies of the transportation system. Furthermore, these models don't adequately consider the transportation network under various scenarios, e.g., link capacity reduction due to traffic accidents or lane closures due to maintenance. Besides, they don't fully investigate the model performance under the situations of incomplete/missing OD demand information. Moreover, how these models perform under out-of-distribution data is not comprehensively explored. These limitations highlight the need for further research to enhance the adaptability and real-world applicability of GNNs for traffic assignment problems.

It should be noted that in the transportation network, a direct link between the origin and destination nodes in general may not exist. This while the traffic flows do in fact depend on the relationship between the OD pairs and OD demands. This observation motivates us to consider introducing the auxiliary links between the origin and destination nodes within the original transportation network, which could encapsulate valuable supplementary information, which is often neglected in the previous literature. In this paper, we propose a novel heterogeneous GNN model for efficient traffic assignment. In addition to roadway links, our model includes virtual links between origin-destination nodes, enriching the model with comprehensive OD demand information and thereby facilitating enhanced feature propagation across the network. Furthermore, we introduce a novel adaptive graph attention mechanism to propagate the node features efficiently. And, the proposed model transforms node embeddings into link embeddings for link flow and flow-capacity ratio estimations. To summarize, the major contributions of this work are as follows: (1) This is the first GNN learning of UE-TAP that integrates interdependencies between origin and destination nodes via a heterogeneous graph structure that consists of physical and virtual links and an adaptive attention-based mechanism; (2) the proposed model is trained using data and the governing conservation law and as such the estimated flows are more accurate; (3) due to the integration of virtual links and regularization based on the conservation law, the performance on unseen graphs is improved. The efficiency and generalization capability of the proposed model are investigated through multiple experiments with different road network topologies, link characteristics, and OD demands.

The remainder of this article is structured as follows. General backgrounds on the traffic assignment

problem, the neural network and graph neural network models are presented in Section 2. Section 3 includes the explanation of the proposed heterogeneous graph neural network for traffic assignment and traffic flow learning. Furthermore, the experiments with urban road networks and generalized synthetic networks are presented to demonstrate the accuracy and generalization capability of the proposed framework in Section 4. Finally, the conclusion and discussion of the proposed framework are presented in Section 5.

## 2. Technical Background

### 2.1. Traffic Assignment Problem

The traffic assignment problem involves assigning traffic volumes or flows to each edge in the network. Given a transportation network represented as a graph  $\mathcal{G} = (\mathcal{V}, \mathcal{E})$ , where nodes  $\mathcal{V}$  represent intersections of roads and edges  $\mathcal{E}$  represent roads or links connecting these locations, The general form of traffic assignment problem can be considered as an optimization task:

$$\min_f : \sum_{e \in \mathcal{E}} Z_e(f_e), \quad (1)$$

where  $f_e$  and  $Z_e(f_e)$  are the total flow and the link cost function on link  $e$ , respectively. The link cost function can be expressed as the function of travel time, travel distance, or other relevant factors. Besides, the traffic assignment problem can have different formulations depending on the specific objectives and assumptions. For instance, the (Beckmann et al., 1956) addresses the user equilibrium traffic assignment problem by optimizing the following objective function:

$$\begin{aligned} \min : \quad & z(x) = \sum_{e \in \mathcal{E}} \int_0^{x_e} t_e(\omega) d\omega \\ \text{s.t.} \quad & \sum_k f_k^{rs} = q_{rs}, \quad \forall r, s \in \mathcal{V}, \\ & f_k^{rs} \geq 0, \quad \forall k, r, s \in \mathcal{V}, \\ & x_e = \sum_{rs} \sum_k f_k^{rs} \zeta_{e,k}^{rs}, \quad \forall e \in \mathcal{E}, \end{aligned} \quad (2)$$

where the objective function is the summation over all road segments of the integral of the link travel time function between 0 and the link flow.  $t_e(\cdot)$  is the link travel time function,  $q_{rs}$  is the total demand from source  $r$  to destination  $s$ ,  $f_k^{rs}$  represents the flow on  $k^{\text{th}}$  path from  $r$  to  $s$ .  $\zeta_{e,k}^{rs}$  is the binary value, which equals 1 when link  $e$  is on  $k^{\text{th}}$  connecting  $r$  and  $s$ . It is noted that the objective function in Beckmann's formulation serves more as a mathematical construct for optimization than a direct physical representation. Compared with UE-TAP, SO-TAP changes the objective function to the summation of the travel time of all vehicles, which reflects a system-optimized perspective.

### 2.2. Neural Networks

Without loss of generality, we will start by considering a neural network with only one layer. Given a  $p$ -dimensional input vector  $h^k \in \mathbb{R}^p$ ,  $q$ -dimensional the output  $h^{k+1} \in \mathbb{R}^q$  of single layer neural network, The single-layer neural network with index  $k$  can be expressed as:

$$h^{k+1} = \sigma(h^k \mathbf{W}_k + \mathbf{b}_k), \quad (3)$$

where  $\mathbf{W}_k \in \mathbb{R}^{p \times q}$  and  $\mathbf{b}_k \in \mathbb{R}^{1 \times q}$  represent the weight and bias term, respectively. The non-linear activation function  $\sigma(\cdot)$  is utilized in the neural network. Theoretically, a single-layer neural network with an infinite number of neurons can approximate any continuous function to arbitrary accuracy, given a sufficiently large dataset (Hornik et al., 1989). However, due to limitations in network width, dataset size, and the challenge of tuning parameters, a single-layer network is not optimal for achieving top performance, which leads to overfitting and poor generalization performance. To alleviate the limitation, multiple neural network layers are stacked together to enhance its expressibility and capture complex hierarchical features.

### 2.3. Graph Neural Network

Neural networks have shown remarkable performance in various applications. In most neural network applications, input data structures are normally fixed, which is also called Euclidean data. However, non-Euclidean data structure such as graph-structured data is pervasive in different applications. The complexity and variability of the graph structure data make it difficult to model with conventional neural network architectures. To address this challenge, GNNs are specifically designed to handle graph-structured data. It operates on the node features and edge features and learns to extract embedding from nodes and edges, aiming to capture the underlying graph structure.

There are different types of graph neural network formulation. One of the popular approaches is the spectral approach (Wang and Zhang, 2022). Spectral graph convolution is a type of convolution operation on graph signals that uses the graph Fourier transform. It operates in the frequency domain and utilizes the eigenvalues and eigenvectors of the graph Laplacian to filter the node features. Given a graph  $\mathcal{G} = (\mathcal{V}, \mathcal{E})$  with adjacency matrix  $\mathbf{A}$  and diagonal degree matrix  $\mathbf{D} = \text{diag}(\mathbf{A}\mathbf{1})$ , the Laplacian matrix and normalized Laplacian matrix of the graph is defined as  $\mathbf{L} = \mathbf{D} - \mathbf{A}$  and  $\mathbf{L}_{\text{norm}} = \mathbf{D}^{-\frac{1}{2}}\mathbf{L}\mathbf{D}^{-\frac{1}{2}}$ , respectively. The spectral graph convolution is defined mathematically as:

$$g_{\theta} * \mathbf{x} = \mathbf{U}g_{\theta}(\mathbf{U}^T \mathbf{x}), \quad (4)$$

where  $g_{\theta}$  is a filter with learnable parameters  $\theta$ ,  $\mathbf{x} \in \mathbb{R}^{|\mathcal{V}| \times N_F}$  is the input features with  $|\mathcal{V}|$  nodes and  $N_F$  features per node, and  $\mathbf{U}$  is the eigenvectors of  $\mathbf{L}_{\text{norm}}$ . The input signal is first transformed into the spectral domain. The features are passed through the learnable filter and transformed back into the spatial domain. The graph spectral operator can be applied to graphs of varying sizes. As a different approach to modeling graph data, the graph attention network (GAT) learns the graph feature by computing attention scores for each node based on its features and the features of its neighbors (Veličković et al., 2017). The graph attention network computes the new node representation  $\mathbf{x}'_i$  for each node  $i$  as follows:

$$\mathbf{x}'_i = \sigma \left( \sum_{j=1}^N \alpha_{ij} \mathbf{W}_x \mathbf{x}_j \right), \quad (5)$$

where  $\sigma$  is an activation function,  $\mathbf{W}_x$  is a learnable weight matrix, and  $\alpha_{ij}$  is the attention weight assigned to the node  $j$  related to its neighbour node  $i$ . The attention weights are computed as follows:

$$\alpha_{ij} = \frac{\exp(\sigma(\mathbf{a}^T[\mathbf{W}_x \mathbf{x}_i \oplus \mathbf{W}_x \mathbf{x}_j]))}{\sum_{k \in \mathcal{N}(i)} \exp(\sigma(\mathbf{a}^T[\mathbf{W}_x \mathbf{x}_i \oplus \mathbf{W}_x \mathbf{x}_k]))}, \quad (6)$$

where  $\mathbf{a}$  is a learnable weight vector,  $\mathcal{N}(i)$  is the set of neighboring nodes of node  $i$ ,  $\oplus$  denotes concatenation function. The graph attention mechanism can be stacked into multiple layers, with each layer learning increasingly complex representations of the graph. The attention mechanism allows the network to learn the different importance of different nodes within a neighborhood, which can improve model performance.

The aforementioned formulation is valid for homogeneous graphs, where all nodes and edges have the same semantic meaning. However, it is noted that real-world graphs are not always homogeneous. For instance, in the literature citation graph, nodes can represent various entities such as papers, authors, and journals, while edges may denote different semantic relationships. When the graph contains different types of nodes or edges, it is considered as a heterogeneous graph. Utilizing GNNs on heterogeneous graphs offers notable advantages over homogeneous counterparts, particularly in the ability to learn type-specific representations for each node and edge type (Wang et al., 2019b; Fu et al., 2020). This allows for more accurate and targeted modeling of each entity and relationship, leading to improved performance on downstream tasks (Zhao et al., 2021). In the following sections, we will leverage the expressiveness of the heterogeneous graph neural network to estimate the traffic flow performance under different OD demand settings.

### 3. Traffic Assignment and Traffic Flow Learning using Heterogeneous Graph Neural Networks

In this section, we elaborate on the proposed architecture of the heterogeneous graph neural networks for traffic assignment and traffic flow learning. The illustration of the proposed model is shown in Fig. 1. It consists of three modules: graph construction & feature preprocessing module; spatial feature extraction module, and edge prediction module. The detail explanation of each module is described as follows.

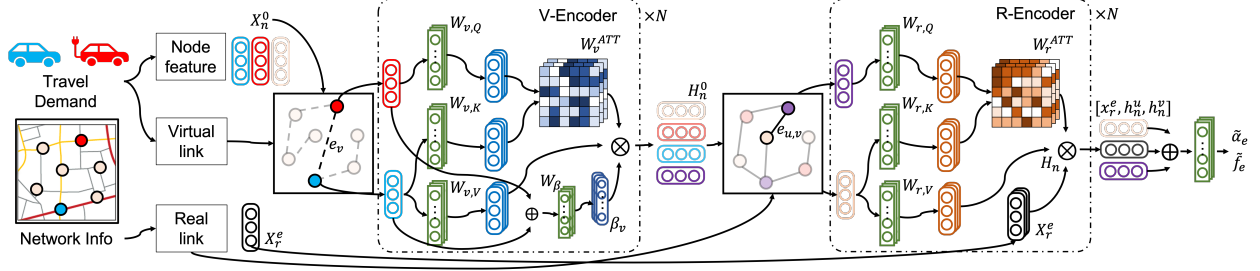


Figure 1: The illustration of the heterogeneous graph neural network for traffic flow learning. The proposed model consists of three parts: graph construction & feature preprocessing module; spatial feature extraction module, and edge prediction module. The graph features are first passed into the virtual encoder (V-Encoder) through the virtual links. Then the graph embeddings are passed into the real encoder (R-Encoder) through the real links. The flow-capacity ratio and link flow of each link are calculated using the source node feature, destination node feature, and normalized edge feature.

### 3.1. Graph Construction & Feature Preprocessing

The heterogeneous graph  $\mathcal{G} = (\mathcal{V}, \mathcal{E}_r, \mathcal{E}_v)$  for traffic flow learning consists of one type of node representing the intersections of road segments and two edge types: real links and virtual links. The real links represent the road segments in the road network, while the virtual links represent the auxiliary link between the origin and destination nodes. The incorporation of the virtual link, as an edge augmentation technique, is strategically employed to facilitate enhanced feature updating. In this model, the node feature attribute is denoted as  $\mathbf{X}_n \in \mathbb{R}^{|\mathcal{V}| \times (|\mathcal{V}|+2)}$ , where  $\mathcal{V}$  represents the graph's node set. Specifically, each row  $\mathbf{x}_u \in \mathbb{R}^{1 \times (|\mathcal{V}|+2)}$  within this matrix corresponds to the feature vector of a single node  $u \in \mathcal{V}$  including the origin-destination demand as well as geographical coordinates. The feature representation for the entire set of real edges is represented with  $\mathbf{X}_{e,r} \in \mathbb{R}^{|\mathcal{E}_r| \times 2}$ . Each row in this matrix includes the free-flow travel time and the link capacity for a single link.

Furthermore, the original node features are often sparse and non-normalized. To address this issue, we employ a preprocessing step to encode the raw features into a lower-dimensional representation. This process not only captures the essential attributes of the data but also retains the semantic information. The generated node feature embedding size is  $\mathbf{X}_n^0 \in \mathbb{R}^{|\mathcal{V}| \times N_v}$ , where  $N_v$  is the embedding size. Similarly, the edge features are also normalized before being propagated in the message passing. Additionally, it should be noted that there is an overlap between the real links and virtual links in the heterogeneous graph because it is possible that a road and an OD demand both exist between the same node pair.

### 3.2. Graph Spatial Features Extraction

As discussed in Section 2.3, the key challenge in heterogeneous graphs lies in effectively aggregating diverse node and edge information. To address this challenge, we propose a novel sequential graph encoder for feature extraction and propagation. The sequential graph encoder is twofold: virtual graph encoder (V-Encoder) and real graph encoder (R-Encoder). Each part leverages attention mechanisms tailored to either virtual or real links, respectively. We will elaborate on these components in the following sections.

#### 3.2.1. Virtual Graph Encoder (V-Encoder)

As the first step of spatial feature extraction, we employ a graph transformer-based attention mechanism on graph features to enhance the modeling capability. Specifically, we transform node features into key, query, and value matrices and then calculate the attention score between node pairs. Furthermore, since the virtual links are synthetically generated without inherent edge features, we introduce a learnable adaptive weight for virtual links, serving as their edge features. The adaptive weight for each node pair is derived by concatenating the two node features and passing through a position-wise feed-forward network (FFN). Mathematically,  $L^{\text{th}}$  V-Encoder can be expressed as:

$$\begin{aligned}
\mathbf{q}^{L,i}, \mathbf{k}^{L,i}, \mathbf{v}^{L,i} &= \mathbf{x}_u^L [\mathbf{W}_q^{L,i}, \mathbf{W}_k^{L,i}, \mathbf{W}_v^{L,i}], & \forall u \in \mathcal{V} \\
\beta_e^{L,i} &= \text{FFN} \left( [\mathbf{x}_u^{L,i} \oplus \mathbf{x}_v^{L,i}]; \mathbf{W}_\beta^{L,i}, \mathbf{b}_\beta^{L,i} \right), & \forall e = (u, v) \in \mathcal{E}_v \\
s_e^{L,i} &= \exp \left( \frac{\mathbf{q}_u^{L,i} \mathbf{k}_v^{L,i}}{\sqrt{d_L}} \beta_e^{L,i} \right), & \forall e = (u, v) \in \mathcal{E}_v
\end{aligned} \tag{7}$$

where  $\mathbf{x}_u^L$  is the feature embedding of node  $u \in \mathcal{V}$  at  $L^{\text{th}}$  layer of V-Encoder.  $\mathbf{q}_{(\cdot)} \in \mathbb{R}^{d_L}$ ,  $\mathbf{k}_{(\cdot)} \in \mathbb{R}^{d_L}$ , and  $\mathbf{v}_{(\cdot)} \in \mathbb{R}^{d_L}$  is the query, key, and value vector at  $i^{\text{th}}$  head in V-Encoder where  $d_L$  denotes the dimensionality of the feature vectors.  $\mathbf{W}_{(\cdot)}$  and  $\mathbf{b}_{(\cdot)}$  is the learnable parameters.  $\beta_e^{L,i} \in \mathbb{R}$  and  $s_e^{L,i} \in \mathbb{R}$  represents the learnable adaptive weight and the unnormalized attention score of the edge  $e = (u, v) \in \mathcal{E}_v$  at  $i^{\text{th}}$  head of  $L^{\text{th}}$  layer, respectively.  $\oplus$  is the concatenation operator. The introduction of edge-level adaptive weights is motivated by the fact that the observed variability in low-dimensional node embedding, in turn reflects the variability in node OD demand. Specifically, node pairs with higher OD demands should receive higher attention scores since they have more significant impacts on the flow distribution. By introducing the adaptive edge-level weight, the graph encoder can adjust the attention score among these node pairs and adaptively propagate the most relevant information through virtual links, thereby enriching the model's contextual understanding. Then value vectors normalized by the attention scores, are processed through another position-wise feed-forward network, accompanied by layer normalization. Additionally, a residual connection supplements the final output of the layer, ensuring the integration of original input features with learned representations for enhanced model performance. Finally, the output of the V-encoder is obtained by concatenating the outputs from all attention heads:

$$\begin{aligned}
\mathbf{z}_u^{L,i} &= \sum_{v \in \mathcal{N}_o(u)} s_{(u,v)}^{L,i} \mathbf{v}_v^{L,i} / \sum_{v \in \mathcal{N}_o(u)} s_{(u,v)}^{L,i}, \\
\mathbf{x}_u^{L+1,i} &= \mathbf{x}_u^{L,i} + \text{LayerNorm} \left( \text{FFN} \left( \mathbf{z}_u^{L,i}; \mathbf{W}_z^{L,i}, \mathbf{b}_z^{L,i} \right) \right), & \forall u \in \mathcal{V} \\
\mathbf{x}_u^{L+1} &= [\mathbf{x}_u^{L+1,0} \oplus \mathbf{x}_u^{L+1,1} \oplus \dots \oplus \mathbf{x}_u^{L+1,N_h}],
\end{aligned} \tag{8}$$

where  $\mathbf{z}_u^{L,i}$  represents the normalized weighted vector of node  $u$  and  $\mathcal{N}_o(u)$  represents all the outgoing nodes connected to  $u$ .  $N_h$  represents the number of attention heads of the V-Encoder. To enhance the propagation of node features throughout the network, we sequentially stack multiple layers of the V-Encoder. The final output of this stacked V-Encoder, denoted as  $H_n^0$ , serves as the input for the subsequent encoder.

### 3.2.2. Real Graph Encoder (R-Encoder)

The R-Encoder is designed to enhance and complement the functionality of the V-Encoder. These two encoders share a similar architecture but slightly differ in the graph attention score mechanism. To illustrate, some nodes in the V-Encoder do not exchange messages with others due to the absence of virtual link connections. The R-Encoder addresses this issue by updating node features through real links, ensuring a comprehensive assessment of direct and indirect node relationships. From a mathematical perspective, the  $M^{\text{th}}$  layer of R-Encoder is expressed as follows:

$$\begin{aligned}
\mathbf{q}^{M,j}, \mathbf{k}^{M,j}, \mathbf{v}^{M,j} &= \mathbf{h}_u^M [\mathbf{W}_q^{M,j}, \mathbf{W}_k^{M,j}, \mathbf{W}_v^{M,j}], & \forall u \in \mathcal{V} \\
s_e^{M,j} &= \exp \left( \sum_{p=1}^P \frac{\mathbf{q}_u^{M,j} \mathbf{k}_v^{M,j}}{\sqrt{d_L}} \beta_{e,p}^r \right), & \forall e = (u, v) \in \mathcal{E}_r \\
\mathbf{z}_u^{M,j} &= \sum_{v \in \mathcal{N}_o(u)} s_{(u,v)}^{M,j} \mathbf{v}_v^{M,j} / \sum_{v \in \mathcal{N}_o(u)} s_{(u,v)}^{M,j}, & \forall u \in \mathcal{V} \\
\mathbf{h}_u^{M+1,j} &= \mathbf{h}_u^{M,j} + \text{LayerNorm} \left( \text{FFN} \left( \mathbf{z}_u^{M,j}; \mathbf{W}_z^{M,j}, \mathbf{b}_z^{M,j} \right) \right), & \forall u \in \mathcal{V} \\
\mathbf{h}_u^{M+1} &= [\mathbf{h}_u^{M+1,0} \oplus \mathbf{h}_u^{M+1,1} \oplus \dots \oplus \mathbf{h}_u^{M+1,N_h}], & \forall u \in \mathcal{V}
\end{aligned} \tag{9}$$

where  $\mathbf{h}_u^M$  is the feature embedding of node  $u \in \mathcal{V}$  at  $M^{\text{th}}$  layer of R-Encoder.  $\mathbf{q}_{(\cdot)} \in \mathbb{R}^{d_L}$ ,  $\mathbf{k}_{(\cdot)} \in \mathbb{R}^{d_L}$ , and  $\mathbf{v}_{(\cdot)} \in \mathbb{R}^{d_L}$  is the query, key, and value matrices at  $j^{\text{th}}$  head of R-Encoder.  $\mathbf{W}_{(\cdot)}$  and  $\mathbf{b}_{(\cdot)}$  are the learnable parameters.  $\beta_{e,p}^r$  represents the  $p^{\text{th}}$  normalized edge feature of link  $e \in \mathcal{E}_r$ . Despite the subtle difference in

the attention mechanism, the node features are propagated in two distinct patterns in the V-Encoder and R-Encoder. To illustrate, the V-Encoder captures the long-range dependency between nodes and integrates the contextual information from non-adjacent nodes. On the contrary, the R-Encoder captures the local topological relationships. Compared with the homogeneous graph with only real links, the additional feature propagation through virtual links can be considered as a dimension-reduction technique to reduce the number of hops required for distant nodes to gather messages. Consequently, it requires fewer GNN layers for effective feature aggregation and following edge prediction. Similar to the V-Encoder, the multiple R-Encoder layers are stacked together, and the output of the last R-Encoder  $\mathbf{O}$ , serves as the input for link flow prediction.

### 3.3. Graph Edge Prediction

To predict the traffic flow at the edge level, the node embedding of the source node and destination node, and the normalized real edge feature are concatenated and passed through a feed-forward neural network. In this paper, we consider the flow-capacity ratio  $\tilde{\alpha}_e$  as the quantity of the final link prediction, which is the link flow normalized by the link capacity:

$$\tilde{\alpha}_e = \text{MLP}([\mathbf{o}_u \oplus \mathbf{o}_v \oplus \beta_e^r]; \mathbf{W}_o, \mathbf{b}_o), \quad \forall e = (u, v) \in \mathcal{E}_r \quad (10)$$

where  $\mathbf{o}_{(\cdot)}$  represent the node embedding.  $\mathbf{W}_o$  and  $\mathbf{b}_o$  is the learnable parameters associated with the multilayer perceptron. The predicted link flows  $\tilde{f}_e$  can be calculated by multiplying the link capacity with the predicted flow-capacity ratio. Subsequently, selecting an appropriate loss function becomes crucial to ensure the model's effective convergence. The proposed model employs a composite loss function comprising two components. The first part is the supervised loss, which measures the difference between prediction and ground truth. It considers both the discrepancy from the flow-capacity ratio  $L_\alpha$  and the link flow  $L_f$  on each link:

$$\begin{aligned} L_s &= L_\alpha + L_f \\ &= \frac{1}{|\mathcal{E}_r|} \sum_{e \in \mathcal{E}_r} \|\alpha_e - \tilde{\alpha}_e\| + \frac{1}{|\mathcal{E}_r|} \sum_{e \in \mathcal{E}_r} \|f_e - \tilde{f}_e\|, \end{aligned} \quad (11)$$

where the  $\alpha_e$  and  $\tilde{\alpha}_e$  represent the ground truth and prediction of flow-capacity ratio on link  $e \in \mathcal{E}$ . The  $f_e$  and  $\tilde{f}_e$  represent the ground truth and prediction of link flow on link  $e \in \mathcal{E}$ . The second part of the loss function originates from the principle of node-based flow conservation, where the total flow of traffic entering a node equals the total flow of traffic exiting that node. The node-based flow conservation law can be represented mathematically:

$$\sum_k f_{ki} - \sum_j f_{ij} = \Delta f_i = \begin{cases} \sum_{v \in \mathcal{V}} O_{v,i} - \sum_{v \in \mathcal{V}} O_{i,v}, & \text{if } i \in \mathcal{V}_{OD}, \\ 0 & \text{otherwise,} \end{cases} \quad (12)$$

where  $f_{ki}$  denotes the flow on the link  $(k, i)$ ,  $\Delta f_i$  represents the difference between flow receiving and sending at node  $i$ ,  $O_{v,i}$  represents the number of OD demand from  $v$  to  $i$ .  $\mathcal{V}_{OD}$  denote the origin-destination node set. The node-based flow conservation law can be considered as a normalization loss, thereby ensuring compliance with the fundamental principle of flow conservation. One common way to incorporate conservation law into the loss function is to define a residual loss function:

$$L_c = \sum_i \left| \sum_{k \in \mathcal{N}_i(i)} \tilde{f}_{ki} - \sum_{j \in \mathcal{N}_o(i)} \tilde{f}_{ij} - \Delta f_i \right|, \quad (13)$$

where  $\mathcal{N}_i(i)$  represent the incoming edges of node  $i$ . The normalization loss  $L_c$  measures how the flow prediction satisfies the flow conservation law. Minimizing this loss function during training will encourage the model to learn traffic flow patterns that satisfy the conservation law. Consequently, the total loss for the flow prediction  $L_{total}$  is the weighted summation of the supervised loss and the conservation loss:

$$L_{total} = w_\alpha L_\alpha + w_f L_f + w_c L_c, \quad (14)$$

where the  $w_\alpha$ ,  $w_f$  and  $w_c$  represent the normalized weight for supervised loss of flow-capacity ratio, supervised loss of actual flow, and the conservation loss, respectively.

## 4. Numerical Experiments

Two numerical experiments are conducted to evaluate the accuracy, efficiency, and generalization capability of the proposed graph neural network. The first experiment is on urban transportation networks. The second experiment is on multiple synthetic graphs with different topologies. The details of the experiments will be explained in the following sections.

Table 1: The detail of urban transportation network. Three networks, including Sioux Falls, East Massachusetts, and Anaheim, are considered.

Network Name	$ \mathcal{V} $	$ \mathcal{E} $	Average Degree	OD Demand
Sioux Falls	24	76	3.17	188,960
EMA	74	258	3.49	132,106
Anaheim	416	914	3.05	226,279

### 4.1. Experiments on Urban Transportation Networks

As case studies, three urban transportation networks are selected: Sioux Falls network, East Massachusetts Network (EMA), and Anaheim network. The information about the network topology, link characteristics, and the OD demand of these networks are obtained from (Bar-Gera et al., 2023). The statistics and the illustration of the network topologies are shown in Table 1 and Figure 2, respectively. To create demand variation, we scaled the demand by a scaling factor according to

$$\tilde{O}_{s,t} = \delta_{s,t}^o O_{s,t}, \quad (15)$$

where  $O_{s,t}$  is the default OD demand between source  $s$  and destination  $t$  and  $\delta_{s,t}^o \sim U(0.5, 1.5)$  is the uniformly distributed random scaling factor for the OD pair  $(s, t)$ . Additionally, to account for variations in network properties, variable link capacities are created according to

$$\tilde{c}_a = \delta_a^c c_a, \quad (16)$$

where  $c_a$  is the original link capacity for link  $a$ , and  $\delta_a^c$  is the scaling factor for link  $a$ . Capacity variations are considered to be due to traffic accidents, road construction/damage, and adverse weather conditions, which reduce the link capacity. In this work, three levels of capacity reduction are considered: (L): light disruption with  $\delta_a^c \sim U(0.8, 1.0)$ ; (M) moderate disruption with  $\delta_a^c \sim U(0.5, 1.0)$ ; (H) high disruption with  $\delta_a^c \sim U(0.2, 1.0)$ .

The size of the dataset for each network at each disruption scenario is 5000, which is split into the training set and the testing set with a ratio of 80% and 20%, respectively. To demonstrate the dataset is sufficiently diverse to cover enough scenarios, the coefficient of variation of network link capacity and OD demand is calculated and the histogram of the link capacity and the OD demand of training and testing data is shown in Figure 3. The OD demand of each network is normalized to 100 in order to facilitate a standardized comparison across different networks regardless of their actual size or demand volumes. The minimum coefficient of variation of link capacity and OD demand among the three networks is 0.45 and 0.22, respectively, which indicates the training and testing data are sufficiently diverse to cover different scenarios (Bedeian and Mossholder, 2000; Campbell et al., 2010).

The training and testing dataset are obtained by solving UE-TAP with the Frank-Wolfe algorithm (Fukushima, 1984). The algorithm converges when the square root of the sum of the squared differences between the link flow in two successive iterations, normalized by the sum of the values of the link flow, falls below the threshold of  $1e-5$ . The GNN model is implemented using PyTorch (Paszke et al., 2019) and DGL (Wang et al., 2019a). The preprocessing layer consists of a three-layer fully connected neural network with an embedding size of 32. The number of GNN layers in the proposed model is 4, including two V-Encoders and two R-Encoders. The number of heads in the attention block is 8. For hyper-parameter selection, the hidden layer size is chosen as 64, which is common in neural network implementation (Liu and Meidani, 2023c,b). The learning rate and batch size of training are 0.001 and 128, respectively. The weights of  $L_\alpha$ ,  $L_f$ , and  $L_c$  in equation 14 are chosen as 1.0, 0.005, and 0.05, respectively.



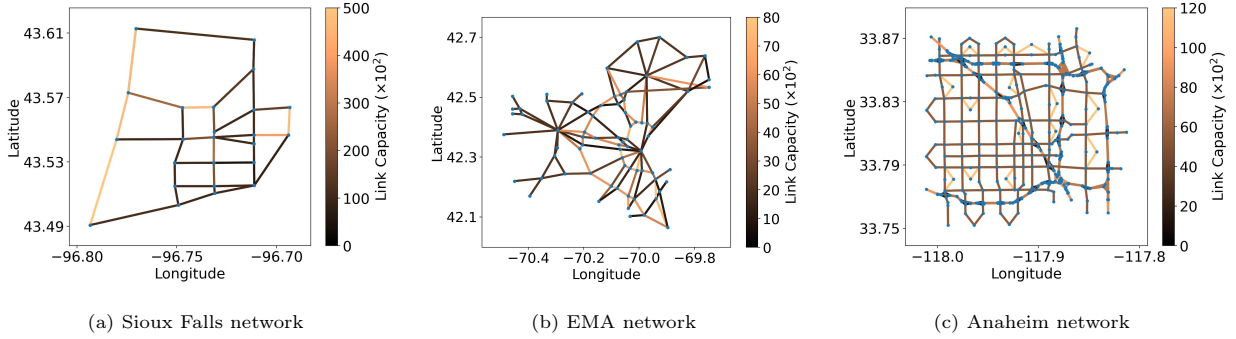


Figure 2: The illustrations of urban transportation networks, including Sioux Falls, EMA, and Anaheim.

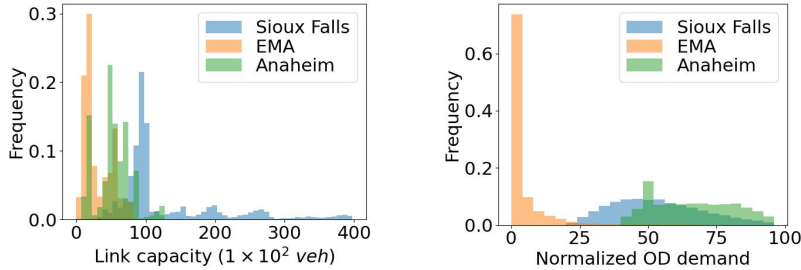


Figure 3: The histogram of the link capacity and OD demand in the training and testing data. Three transportation networks are considered including Sioux Falls, EMA, and Anaheim network.

We evaluated the performance of our proposed heterogeneous GNN model (referred to by HetGAT) and compared it with three benchmark models: a fully connected neural network (FCNN), a homogeneous graph attention network (GAT), and a homogeneous graph convolution network (GCN). The FCNN consisted of five fully connected layers with an embedding size of 64. The GAT and GCN both have four layers of graph message passing layer, followed by three layers of FCNN with an embedding size of 64. The metrics to evaluate performance include the mean absolute error (MAE), root mean square error (RMSE), and the normalized conversation loss  $\tilde{L}_c$ :

$$\text{MAE} = \frac{1}{N} \sum_{i=1}^N |y_i - \tilde{y}_i|, \quad (17)$$

$$\text{RMSE} = \sqrt{\frac{1}{N} \sum_{i=1}^N (y_i - \tilde{y}_i)^2}, \quad (18)$$

$$\tilde{L}_c = \frac{\sum_i |\sum_{k \in \mathcal{N}_i(i)} \tilde{f}_{ki} - \sum_{j \in \mathcal{N}_o(i)} \tilde{f}_{ij} - \Delta f_i|}{\sum_s \sum_t \tilde{O}_{s,t}}, \quad (19)$$

where  $y$  and  $\tilde{y}$  respectively represent the ground truth and predicted values for quantity of interest. We conducted a 5-fold cross-validation for each experiment to ensure the robustness of our results across different subsets of the data.

The training histories of the studied models are shown in Figure 4. The results indicate that the FCNN model performed poorly during training compared to GNN-based models, as shown by the high training loss and early stagnation. In contrast, GCN and GAT models exhibited similar convergence rates. Our proposed model outperformed both GCN and GAT in terms of training loss. Especially when used for larger networks, the proposed model demonstrated superior convergence performance compared to GCN and GAT; for the Anaheim network, the training loss of the proposed model is almost 1/3 of that of GAT in the first

25 iterations. This is because GCN and GAT only consider homogeneous edges, which limits the message passing to adjacent nodes. In contrast, the proposed GNN model uses virtual links and provides augmented connectivity to long-hop node pairs, which makes the node feature updating in HetGAT more efficient.

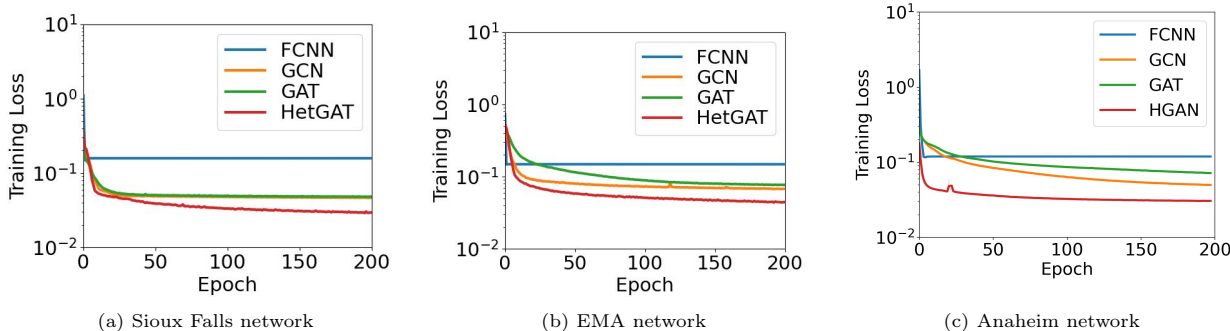


Figure 4: Training loss history under urban transportation network. Three benchmarks, including FCNN, GCN, and GAT, are compared with HetGAT.

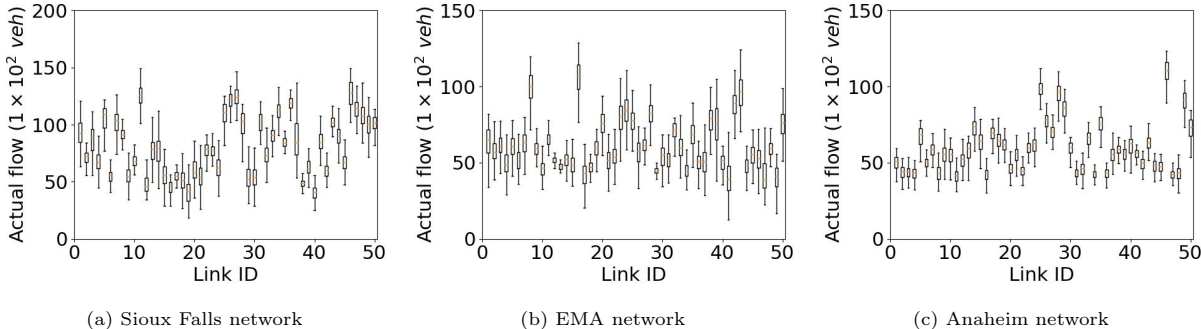


Figure 5: Illustrations of the link-wise flow distribution for different transportation networks. Three transportation networks under major disruption are considered, including Sioux Falls, EMA, and Anaheim networks. 50 links are selected for each network.

After the training is finished, the model performance is evaluated on the testing set. The experiments under the urban road network are conducted in three different settings. The first setting, referred to as LMH-LMH, involved using all levels of disruption (flow reduction scaling levels) in both the training and testing sets. The second setting, namely L-M, involves training the model on light disruption data and testing it on medium disruption data. The third case, which is labeled as M-H, involves training on medium disruption data and testing on high disruption data. The L-M and M-H scenarios will therefore involve unseen cases that don't exist in the training data. Figure 5 visualizes the variations in link-wise flow in Sioux Falls, EMA, and Anaheim networks under high disruption. The average coefficients of variation of actual link flow for three networks are 0.297, 0.242, and 0.201, respectively. Figure 6 plotted the predicted value and ground truth of the flow-capacity ratio on multiple samples in the Anaheim network under the LMH-LMH setting. In total, the flow-capacity ratio on 10,000 edges is predicted using HetGAT, GAT, and GCN, respectively. Figure 6 indicates that HetGAT has a relatively higher correlation coefficient, which outperforms GAT and GCN.

Table 2 summarizes the prediction performance of all methods under different settings, and shows that HetGAT, compared to other models, offers better performance. When the graph size increases, the proposed model maintains a relatively low MAE compared to GCN and GAT. For instance, in the EMA network, HetGAT offers flow MAEs that are 39.5%, 56.4%, and 38.8% lower than the second best result, in LMH-LMH, L-M, and M-H settings, respectively. In the Anaheim network, HetGAT offers flow MAEs that are 27.2%, 47.4%, and 33.1% lower than the second-best result in LMH-LMH, L-M, and M-H settings, respectively. This shows that the inclusion of virtual links can assist GNN models in better learning the traffic flow patterns. In

addition to the prediction accuracy, the training time is also an important factor in evaluating the efficiency and practicality of machine learning models. The computational time is mainly threefold: time for solving UE-TAP, GNN training time, and GNN inference time. For Sioux Falls, EMA, and Anaheim networks, the time for solving UE-TAP is 56.8, 575.2, and 2612.5 min, respectively. In comparison, the training time of HetGAT is 26.8, 28.9, and 59.7 min, respectively. Moreover, for every 1000 graphs, the inference time of the proposed model is notably efficient at 0.13, 0.15, and 0.31 min, respectively. The computational time of each component demonstrates the computational efficiency of the proposed model for solving traffic assignment problems.

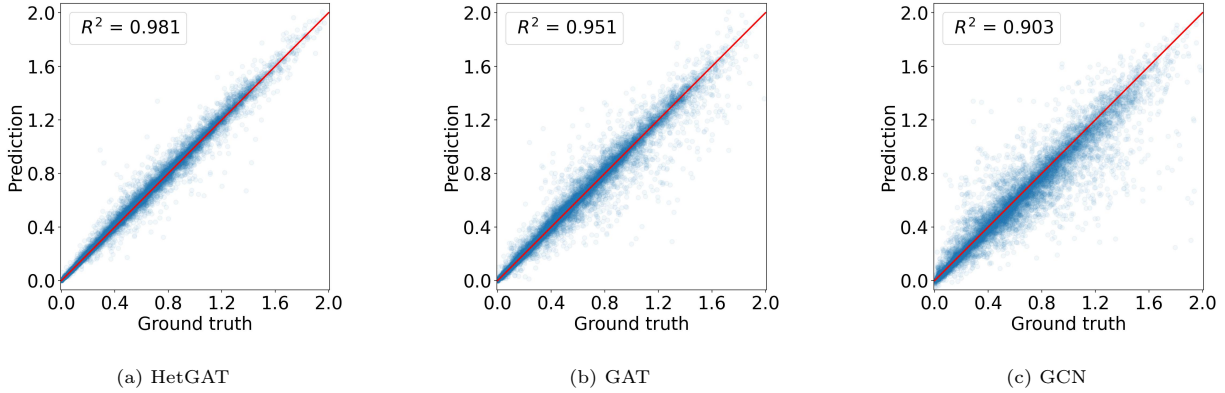


Figure 6: Comparison of predicted flow-capacity ratio between ground truth and surrogate modeling in the Anaheim network under LMH-LMH setting.

Table 2: Performance comparison of HetGAT with benchmark methods. Three different settings are included: LMH-LMH, L-M, M-H. The mean absolute error, root mean square error, and normalized conservation loss are used to evaluate the prediction performance on the testing set.

Network	Model	LMH-LMH					L-M					M-H				
		Flow ( $1 \times 10^2$ )		Link utilization		$\tilde{L}_c$	Flow ( $1 \times 10^2$ )		Link utilization		$\tilde{L}_c$	Flow ( $1 \times 10^2$ )		Link utilization		$\tilde{L}_c$
		MAE	RMSE	MAE	RMSE		MAE	RMSE	MAE	RMSE		MAE	RMSE	MAE	RMSE	
Sioux Falls	FCNN	19.31	30.22	16.29%	26.39%	0.38	18.64	27.31	15.87%	24.55%	0.37	32.85	48.08	30.09%	44.99%	0.70
	GCN	5.62	8.80	4.78%	7.74%	0.11	5.43	7.95	4.62%	7.15%	0.14	9.57	14.00	8.64%	12.87%	0.22
	GAT	5.60	8.75	4.74%	7.68%	0.11	5.54	8.18	4.62%	7.15%	0.11	9.55	13.99	8.76%	13.10%	0.20
	HetGAT	<b>3.58</b>	<b>5.56</b>	<b>2.99%</b>	<b>4.74%</b>	<b>0.07</b>	<b>3.73</b>	<b>5.39</b>	<b>2.99%</b>	<b>4.36%</b>	<b>0.07</b>	<b>7.01</b>	<b>10.39</b>	<b>6.32%</b>	<b>9.52%</b>	<b>0.08</b>
EMA	FCNN	7.51	14.82	25.56%	63.89%	0.81	9.04	17.70	32.36%	61.87%	0.46	13.82	24.68	60.47%	122.94%	0.62
	GCN	1.99	3.92	7.62%	18.32%	0.17	2.39	4.69	7.78%	14.65%	0.08	3.66	6.53	14.35%	30.33%	0.12
	GAT	1.77	3.62	6.77%	16.91%	0.21	2.39	4.69	8.57%	16.38%	0.12	3.83	6.87	16.01%	32.54%	0.17
	HetGAT	<b>0.98</b>	<b>2.21</b>	<b>3.48%</b>	<b>8.08%</b>	<b>0.07</b>	<b>1.05</b>	<b>2.06</b>	<b>3.52%</b>	<b>6.85%</b>	<b>0.03</b>	<b>2.49</b>	<b>4.79</b>	<b>9.24%</b>	<b>20.50%</b>	<b>0.07</b>
Anaheim	FCNN	10.61	16.73	24.72%	45.03%	0.81	15.82	28.59	38.44%	69.66%	0.23	18.74	29.82	49.70%	84.45%	0.25
	GCN	2.18	3.44	6.54%	11.53%	0.29	3.25	5.88	9.31%	17.09%	0.07	3.85	6.13	12.37%	20.74%	0.08
	GAT	1.47	2.55	4.77%	8.69%	0.16	2.32	4.18	7.42%	13.45%	0.05	3.31	5.14	9.59%	16.30%	0.05
	HetGAT	<b>1.04</b>	<b>1.81</b>	<b>2.97%</b>	<b>5.46%</b>	<b>0.08</b>	<b>1.19</b>	<b>1.85</b>	<b>3.31%</b>	<b>5.45%</b>	<b>0.02</b>	<b>2.17</b>	<b>3.37</b>	<b>6.66%</b>	<b>10.85%</b>	<b>0.03</b>

As an additional experiment, we consider a realistic scenario where the regional OD demand values are incomplete by introducing a random binary mask to the original OD demand. More specifically, given a specific missing ratio, we randomly select a number of OD pairs and mask their corresponding OD demand values as zeros in the input node feature. In this way, the model is expected to learn the inherent patterns and structures of the transportation network, even when some of the demand information is missing. The effectiveness of the proposed model under incomplete OD demand scenarios will be evaluated by comparing the predicted traffic flows against the ground truth data obtained from the complete OD demand. Three missing ratios are considered in the experiment: 20%, 30%, and 40%. The training setting and the hyperparameters remain the same as those in the aforementioned experiments. Table 3 summarizes the results of prediction performance under different missing rate scenarios for the LMH-LMH setting. The FCNN model is not considered in these experiments because of their very poor performance in the previous experiments under full

OD demand. HetGAT still outperforms GAT and GCN under different networks and different missing ratios. additionally, the flow predictions by HetGAT have relatively better compliance with the flow conservation law compared with GAT and GCN.

Table 3: Comparison of the performance of HetGAT with benchmark under incomplete OD demand. Three missing ratios are considered in the experiments: 20%, 30%, and 40%. The mean absolute error, root mean square error, and normalized conservation loss, are used to evaluate the prediction performance on the testing set.

Network	Model	Missing ratio = 20%					Missing ratio = 30%					Missing ratio = 40%				
		Flow ( $1 \times 10^2$ )		Link utilization		$\tilde{L}_c$	Flow ( $1 \times 10^2$ )		Link utilization		$\tilde{L}_c$	Flow ( $1 \times 10^2$ )		Link utilization		$\tilde{L}_c$
		MAE	RMSE	MAE	RMSE		MAE	RMSE	MAE	RMSE		MAE	RMSE	MAE	RMSE	
Sioux Falls	GCN	6.50	10.00	5.39%	8.62%	0.15	6.54	10.02	5.72%	9.19%	0.15	7.54	11.06	6.68%	10.60%	0.16
	GAT	6.64	10.11	5.83%	9.25%	0.14	7.19	10.50	6.11%	9.45%	0.14	6.68	10.13	5.78%	9.20%	0.15
	HetGAT	<b>4.05</b>	<b>6.04</b>	<b>3.33%</b>	<b>5.06%</b>	<b>0.08</b>	<b>4.13</b>	<b>6.14</b>	<b>3.38%</b>	<b>5.13%</b>	<b>0.09</b>	<b>4.15</b>	<b>6.08</b>	<b>3.45%</b>	<b>5.16%</b>	<b>0.09</b>
EMA	GCN	2.14	4.11	8.06%	16.94%	0.24	2.15	4.10	7.87%	16.47%	0.25	2.14	4.12	8.03%	17.09%	0.26
	GAT	1.87	3.71	6.89%	16.65%	0.18	1.86	3.73	7.00%	16.77%	0.19	1.87	3.73	7.07%	16.97%	0.19
	HetGAT	<b>1.15</b>	<b>2.37</b>	<b>3.98%</b>	<b>8.40%</b>	<b>0.08</b>	<b>1.15</b>	<b>2.37</b>	<b>4.00%</b>	<b>8.24%</b>	<b>0.08</b>	<b>1.21</b>	<b>2.41</b>	<b>4.17%</b>	<b>8.67%</b>	<b>0.09</b>
Anaheim	GCN	2.16	3.38	6.31%	10.86%	0.14	2.24	3.43	6.65%	11.18%	0.14	2.28	3.56	6.82%	11.72%	0.15
	GAT	1.62	2.70	4.80%	8.70%	0.12	1.74	2.85	5.21%	9.34%	0.13	1.68	2.78	4.98%	8.97%	0.12
	HetGAT	<b>1.11</b>	<b>1.91</b>	<b>3.17%</b>	<b>5.78%</b>	<b>0.06</b>	<b>1.08</b>	<b>1.87</b>	<b>3.08%</b>	<b>5.65%</b>	<b>0.05</b>	<b>1.09</b>	<b>1.89</b>	<b>3.12%</b>	<b>5.72%</b>	<b>0.05</b>

#### 4.2. Experiments on Generalized Synthetic Networks

In this section, unlike the experiments in Section 4.1, which involved training and testing on an identical network topology, we examine the generalization capability of the proposed model to networks with varied topologies. In particular, we consider real-world scenarios in which certain links in the network are fully closed due to governmental directives or catastrophic events such as bridge collapses, leading to significant alterations in network topology. Another scenario for topology alternation is when cities consider network expansion to better serve increased mobility demands due to current urbanization trends. Under all these scenarios, the resulting urban networks may exhibit both commonalities and disparities in their topologies (Rodrigue, 2020). This is while training models separately for each distinct network requires substantial time and effort. Motivated by the aforementioned considerations, our aim is to explore the generalization ability of our HetGAT model over varying topologies.

Table 4: Performance comparison of HetGAT with benchmark methods on modified urban transportation network with link addition and removal. The mean absolute error, root mean square error, and normalized conservation loss are used to evaluate the prediction performance on the testing set.

Network	Model	Missing Ratio = 0%					Missing Ratio = 20%					Missing Ratio = 40%				
		Flow ( $1 \times 10^2$ )		Link utilization		$\tilde{L}_c$	Flow ( $1 \times 10^2$ )		Link utilization		$\tilde{L}_c$	Flow ( $1 \times 10^2$ )		Link utilization		$\tilde{L}_c$
		MAE	RMSE	MAE	RMSE		MAE	RMSE	MAE	RMSE		MAE	RMSE	MAE	RMSE	
Sioux	GCN	10.12	13.97	8.31%	11.77%	0.15	10.96	14.82	9.22%	13.05%	0.15	10.94	15.04	9.05%	12.86%	0.15
	GAT	7.16	9.89	6.10%	8.77%	0.13	10.78	14.40	9.11%	12.77%	0.14	12.20	16.42	10.34%	14.58%	0.17
	HetGAT	<b>3.04</b>	<b>4.22</b>	<b>2.56%</b>	<b>3.75%</b>	<b>0.07</b>	<b>3.33</b>	<b>4.53</b>	<b>2.79%</b>	<b>3.96%</b>	<b>0.07</b>	<b>3.46</b>	<b>4.69</b>	<b>2.88%</b>	<b>4.08%</b>	<b>0.08</b>
EMA	GCN	4.60	7.82	15.11%	26.42%	0.26	4.09	6.68	13.97%	24.71%	0.24	4.04	6.57	15.24%	31.99%	0.23
	GAT	2.70	4.50	9.97%	18.21%	0.14	2.73	4.55	10.04%	20.05%	0.15	2.86	4.72	10.50%	19.94%	0.15
	HetGAT	<b>1.28</b>	<b>2.39</b>	<b>4.09%</b>	<b>7.91%</b>	<b>0.06</b>	<b>1.34</b>	<b>2.47</b>	<b>4.29%</b>	<b>8.17%</b>	<b>0.07</b>	<b>1.42</b>	<b>2.57</b>	<b>4.56%</b>	<b>8.42%</b>	<b>0.07</b>
Anaheim	GCN	6.02	9.93	16.29%	26.78%	0.40	5.93	9.83	15.98%	26.40%	0.31	6.04	9.99	16.24%	26.73%	0.37
	GAT	5.43	9.16	14.94%	25.20%	0.25	5.37	9.02	14.83%	25.01%	0.40	5.53	9.28	15.23%	25.60%	0.34
	HetGAT	<b>1.14</b>	<b>2.22</b>	<b>3.29%</b>	<b>6.79%</b>	<b>0.09</b>	<b>1.15</b>	<b>2.08</b>	<b>3.34%</b>	<b>6.49%</b>	<b>0.09</b>	<b>1.29</b>	<b>2.38</b>	<b>3.71%</b>	<b>7.40%</b>	<b>0.10</b>

In this work, we conduct experiments on two sets of networks: (1) modified urban networks of Section 4.1; (2) synthetic networks. The first set, includes networks that are modifications of the original Sioux Falls, EMA, and Anaheim networks by adding and removing links. For each of these networks, we generate 20 unique topological variations. Additionally, we incorporate three configurations of OD demand in our experiments: complete OD setting, 20% and 40% incomplete OD setting. The training setting and the hyperparameters remain the same as those in the aforementioned experiments in Section 4.1. The results are presented in Table 4. It can be seen that compared to the results in Table 2, HetGAT exhibits comparable levels of effectiveness for all networks. Additionally, in comparison to other baseline models, our proposed

HetGAT model consistently outperforms both GAT and GCN over all networks, under both complete and incomplete OD scenarios. It is noteworthy that compared to the homogeneous GNN model, since our model has captured the influence of OD pairs via virtual links, the HetGAT model is more expressive and can better capture and learn the impact of topology alterations on flow distributions.

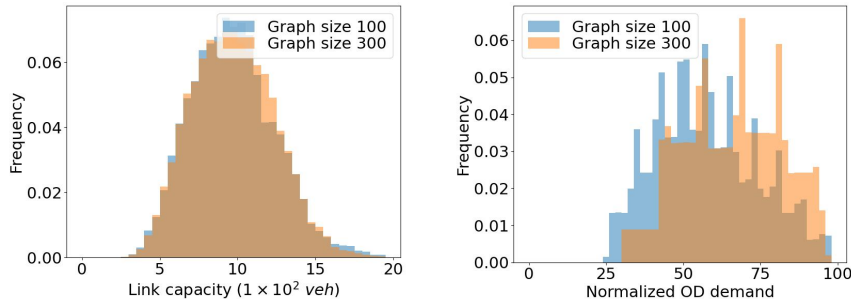


Figure 7: The histogram of the link capacity and normalized OD demand in the training and testing data of synthetic networks. Two sizes of datasets are included: 100 and 300.

The second set includes synthetic networks. We generate these networks by starting with a grid graph and then adding links between randomly selected nodes. Furthermore, to emulate the real road network, a number of nodes and edges are randomly removed until the number of nodes in the graph reaches a predefined threshold. Two sets of synthetic networks are considered: one with 100 nodes and another with 300 nodes. For each graph size, 20 different graph topologies are generated. Three of these randomly generated graphs of size 100 are shown in Figure 8. The OD demand and the link capacity are also randomly generated using the scaling factor according to Equations 15 and 16, respectively. To demonstrate the diversity of these examples, similar to Section 4.1, the histograms of the link capacities and the OD demands in the generated dataset are shown in Figure 7, indicating the training and testing data are sufficiently diverse to cover different scenarios.

In this work, we consider a case in which the training and test graphs are of the same size, and a case where the training and test graphs are of different size (e.g., training graphs of size 100 and test graphs of size 300). It should be noted that the proposed HetGAT involves a node feature whose dimension is equal to the total number of nodes in the graph. Therefore, this requires an adjustment when training and testing are done on graphs with different number of nodes. In addition to standard training, which trains and tests on the same set of graphs, we propose two training strategies, enabling the HetGAT model to be trained and tested effectively on various graphs:

- Transfer learning: we adapt the model trained from previous experiments by substituting the preprocessing and final layers with new parameters, while freezing the remaining parameters unchanged. This facilitates a quick adaption to the new topologies with limited training.
- Homogenized training: we define a maximum node number threshold  $N_{\max}$  and for all the graphs containing fewer nodes than this threshold, we introduce dummy nodes to the graph until the number of node reaches the  $N_{\max}$ . This approach ensures uniform formulation among different graphs, allowing a single model to train and test across graphs of varying sizes.

The training setting and the hyperparameters remain the same as those in the previous experiments. The prediction performance metrics for the testing sets are presented in Table 5. Compared with transfer learning and homogenized learning settings, the proposed model achieves the highest accuracy when same graph size is used in training and testing. Despite a performance decline under the transfer and homogenized learning setting, the HetGAT model maintains a competitive edge, outperforming baseline models such as GAT and GCN.

## 5. Conclusion and Discussion

In this paper, we proposed a novel approach for end-to-end traffic assignment and traffic flow learning using heterogeneous graph neural networks. Compared with conventional homogeneous graph neural networks,

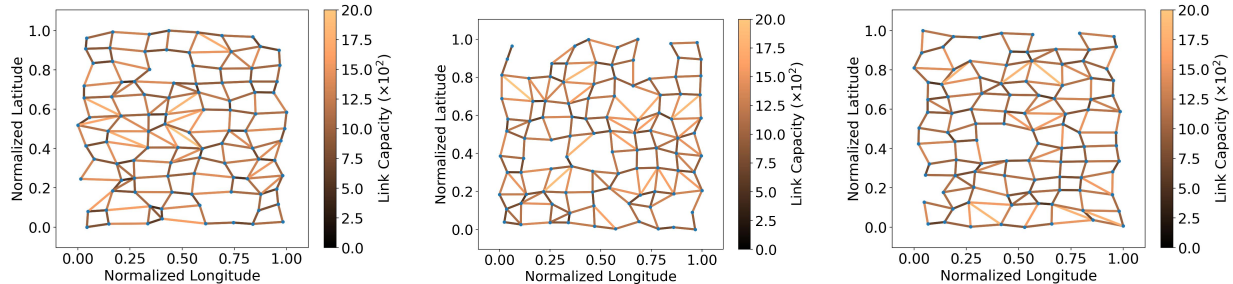


Figure 8: The illustrations of sampled generalized synthetic networks with the network size of 100. The link color represents the link capacity of each link.

Table 5: Comparison of the performance of HetGAT with that of GAT and GCN on generalized synthetic networks. Two graph sizes of 100 and 300 are considered in the experiments. We consider three different training strategies: standard training, transfer learning, and homogenized learning.

Network	Model	Standard training					Transfer learning					Homogenized learning				
		Flow ( $1 \times 10^2$ )		Link utilization		$\bar{L}_c$	Flow ( $1 \times 10^2$ )		Link utilization		$\bar{L}_c$	Flow ( $1 \times 10^2$ )		Link utilization		$\bar{L}_c$
		MAE	RMSE	MAE	RMSE		MAE	RMSE	MAE	RMSE		MAE	RMSE	MAE	RMSE	
100	GCN	1.62	2.40	17.85%	26.89%	0.38	1.82	2.63	20.09%	29.70%	0.10	1.45	2.08	15.76%	23.11%	0.11
	GAT	1.68	2.48	18.40%	27.49%	0.33	1.92	2.79	21.11%	31.30%	0.10	1.63	2.42	17.90%	27.59%	0.11
	HetGAT	<b>0.25</b>	<b>0.38</b>	<b>2.75%</b>	<b>4.27%</b>	<b>0.19</b>	<b>0.38</b>	<b>0.56</b>	<b>4.18%</b>	<b>6.29%</b>	<b>0.09</b>	<b>0.74</b>	<b>1.16</b>	<b>8.46%</b>	<b>14.35%</b>	<b>0.09</b>
300	GCN	2.97	4.11	31.87%	44.14%	0.15	3.09	4.28	33.17%	45.97%	0.13	3.04	4.23	32.65%	45.32%	0.14
	GAT	2.81	3.89	30.10%	41.58%	0.18	2.94	4.05	31.43%	43.33%	0.15	2.85	3.94	30.56%	42.19%	0.16
	HetGAT	<b>0.46</b>	<b>0.69</b>	<b>4.99%</b>	<b>7.51%</b>	<b>0.11</b>	<b>0.78</b>	<b>1.17</b>	<b>8.45%</b>	<b>12.89%</b>	<b>0.06</b>	<b>0.52</b>	<b>0.77</b>	<b>5.63%</b>	<b>8.45%</b>	<b>0.13</b>

we introduce the auxiliary virtual links connecting origin-destination node pairs. Furthermore, we proposed a novel adaptive graph attention mechanism to effectively capture the semantic and contextual features through different types of links. Furthermore, we conducted extensive experiments on three real-world urban transportation networks to evaluate the performance of the proposed model and compared it with the state-of-the-art models. The results indicate that the proposed model outperforms other models in terms of convergence rate and prediction accuracy. Notably, by introducing two different training strategies, the proposed heterogeneous graph neural network model can also be generalized to different network topologies, underscoring its potential in real-world scenarios.

Our work can be considered as an efficient surrogate model for further accelerating the complex optimization tasks including resource allocation and infrastructure asset management. Currently, the proposed HetGAT model only learns and predicts the static traffic flow patterns. As a potential extension of this work, the proposed framework can be extended to learn the dynamic traffic flow patterns. Furthermore, the current proposed GNN model uses training data collected from conventional solvers of static traffic assignment. In future work, we will explore how these models can be trained on traffic data collected from sensors, such as loop detectors, cameras, or GPS devices.

## Acknowledgment

This work was supported in part by the National Science Foundation under Grant CMMI-1752302.

## References

- Bar-Gera, H., Stabler, B., Sall, E., 2023. Transportation networks for research core team. Transportation Network Test Problems. Available online: <https://github.com/bstabler/TransportationNetworks> (accessed on May 14 2023) .
- Beckmann, M., McGuire, C.B., Winsten, C.B., 1956. Studies in the Economics of Transportation. Technical Report.

- Bedeian, A.G., Mossholder, K.W., 2000. On the use of the coefficient of variation as a measure of diversity. *Organizational Research Methods* 3, 285–297.
- Campbell, M.J., Machin, D., Walters, S.J., 2010. *Medical statistics: a textbook for the health sciences*. John Wiley & Sons.
- Di Lorenzo, D., Galligari, A., Sciandrone, M., 2015. A convergent and efficient decomposition method for the traffic assignment problem. *Computational optimization and applications* 60, 151–170.
- Fan, W., Tang, Z., Ye, P., Xiao, F., Zhang, J., 2023. Deep learning-based dynamic traffic assignment with incomplete origin–destination data. *Transportation Research Record* 2677, 1340–1356.
- Fang, J., Qiao, J., Bai, J., Yu, H., Xue, J., 2022. Traffic accident detection via self-supervised consistency learning in driving scenarios. *IEEE Transactions on Intelligent Transportation Systems* 23, 9601–9614.
- Fu, X., Zhang, J., Meng, Z., King, I., 2020. Magnn: Metapath aggregated graph neural network for heterogeneous graph embedding, in: *Proceedings of The Web Conference 2020*, pp. 2331–2341.
- Fukushima, M., 1984. A modified frank-wolfe algorithm for solving the traffic assignment problem. *Transportation Research Part B: Methodological* 18, 169–177.
- Hornik, K., Stinchcombe, M., White, H., 1989. Multilayer feedforward networks are universal approximators. *Neural networks* 2, 359–366.
- Hu, F., Yang, S., Thompson, R.G., 2021. Resilience-driven road network retrofit optimization subject to tropical cyclones induced roadside tree blowdown. *International Journal of Disaster Risk Science* 12, 72–89.
- Kuang, Z., Mazalov, V.V., Tang, X., Zheng, J., 2021. Transportation network with externalities. *Journal of Computational and Applied Mathematics* 382, 113091.
- Liu, T., Meidani, H., 2022. Graph neural network surrogate for seismic reliability analysis of highway bridge system. *arXiv preprint arXiv:2210.06404* .
- Liu, T., Meidani, H., 2023a. Optimizing seismic retrofit of bridges: Integrating efficient graph neural network surrogates and transportation equity, in: *Proceedings of Cyber-Physical Systems and Internet of Things Week 2023*, pp. 367–372.
- Liu, T., Meidani, H., 2023b. Physics-informed neural network for nonlinear structural system identification, in: *14th International Workshop on Structural Health Monitoring: Designing SHM for Sustainability, Maintainability, and Reliability, IWSHM 2023*, DEStech Publications. pp. 3001–3011.
- Liu, T., Meidani, H., 2023c. Physics-informed neural networks for system identification of structural systems with a multiphysics damping model. *Journal of Engineering Mechanics* 149, 04023079.
- Liu, Z., Yin, Y., Bai, F., Grimm, D.K., 2023. End-to-end learning of user equilibrium with implicit neural networks. *Transportation Research Part C: Emerging Technologies* 150, 104085.
- Madadi, B., de Almeida Correia, G.H., 2024. A hybrid deep-learning-metaheuristic framework for bi-level network design problems. *Expert Systems with Applications* 243, 122814.
- Nie, Y., Zhang, H., Lee, D.H., 2004. Models and algorithms for the traffic assignment problem with link capacity constraints. *Transportation Research Part B: Methodological* 38, 285–312.
- Nishi, T., Otaki, K., Hayakawa, K., Yoshimura, T., 2018. Traffic signal control based on reinforcement learning with graph convolutional neural nets, in: *2018 21st International conference on intelligent transportation systems (ITSC)*, IEEE. pp. 877–883.
- Paszke, A., Gross, S., Massa, F., Lerer, A., Bradbury, J., Chanan, G., Killeen, T., Lin, Z., Gimelshein, N., Antiga, L., et al., 2019. Pytorch: An imperative style, high-performance deep learning library. *Advances in neural information processing systems* 32.

- Rahman, R., Hasan, S., 2023. Data-driven traffic assignment: A novel approach for learning traffic flow patterns using graph convolutional neural network. *Data Science for Transportation* 5, 11.
- Rodrigue, J.P., 2020. *The geography of transport systems*. Routledge.
- Seliverstov, Y.A., Seliverstov, S.A., Malygin, I.G., Tarantsev, A.A., Shatalova, N.V., Lukomskaya, O.Y., Tishchenko, I.P., Elyashevich, A.M., 2017. Development of management principles of urban traffic under conditions of information uncertainty, in: *Creativity in Intelligent Technologies and Data Science: Second Conference, CIT&DS 2017, Volgograd, Russia, September 12-14, 2017, Proceedings 2*, Springer. pp. 399–418.
- Silva-Lopez, R., Baker, J.W., Poulos, A., 2022. Deep learning-based retrofitting and seismic risk assessment of road networks. *Journal of Computing in Civil Engineering* 36, 04021038.
- Sun, W., Shao, H., Wu, T., Shao, F., Fainman, E.Z., 2022. Reliable location of automatic vehicle identification sensors to recognize origin-destination demands considering sensor failure. *Transportation research part C: emerging technologies* 136, 103551.
- Tang, K., Cao, Y., Chen, C., Yao, J., Tan, C., Sun, J., 2021. Dynamic origin-destination flow estimation using automatic vehicle identification data: A 3d convolutional neural network approach. *Computer-Aided Civil and Infrastructure Engineering* 36, 30–46.
- Veličković, P., Cucurull, G., Casanova, A., Romero, A., Lio, P., Bengio, Y., 2017. Graph attention networks. *arXiv preprint arXiv:1710.10903* .
- Wang, M., Zheng, D., Ye, Z., Gan, Q., Li, M., Song, X., Zhou, J., Ma, C., Yu, L., Gai, Y., et al., 2019a. Deep graph library: A graph-centric, highly-performant package for graph neural networks. *arXiv preprint arXiv:1909.01315* .
- Wang, X., Ji, H., Shi, C., Wang, B., Ye, Y., Cui, P., Yu, P.S., 2019b. Heterogeneous graph attention network, in: *The world wide web conference*, pp. 2022–2032.
- Wang, X., Zhang, M., 2022. How powerful are spectral graph neural networks, in: *International Conference on Machine Learning*, PMLR. pp. 23341–23362.
- Ye, J., Sun, L., Du, B., Fu, Y., Tong, X., Xiong, H., 2019. Co-prediction of multiple transportation demands based on deep spatio-temporal neural network, in: *Proceedings of the 25th ACM SIGKDD international conference on knowledge discovery & data mining*, pp. 305–313.
- Zhang, J., Che, H., Chen, F., Ma, W., He, Z., 2021. Short-term origin-destination demand prediction in urban rail transit systems: A channel-wise attentive split-convolutional neural network method. *Transportation Research Part C: Emerging Technologies* 124, 102928.
- Zhang, Z., Li, M., Lin, X., Wang, Y., 2020. Network-wide traffic flow estimation with insufficient volume detection and crowdsourcing data. *Transportation Research Part C: Emerging Technologies* 121, 102870.
- Zhao, J., Wang, X., Shi, C., Hu, B., Song, G., Ye, Y., 2021. Heterogeneous graph structure learning for graph neural networks, in: *Proceedings of the AAAI conference on artificial intelligence*, pp. 4697–4705.
- Zhaowei, Q., Haitao, L., Zhihui, L., Tao, Z., 2020. Short-term traffic flow forecasting method with mb-lstm hybrid network. *IEEE Transactions on Intelligent Transportation Systems* 23, 225–235.
- Zou, Q., Chen, S., 2020. Resilience modeling of interdependent traffic-electric power system subject to hurricanes. *Journal of Infrastructure Systems* 26, 04019034.